

Benchmarking DFT and TD-DFT Functionals for the Ground and Excited States of Hydrogen-Rich Peptide Radicals

Vanessa Riffet,[†] Denis Jacquemin,^{‡,§} Emilie Cauët,^{||} and Gilles Frison^{*,†}

[†]Laboratoire de Chimie Moléculaire, Département de Chimie, Ecole polytechnique and CNRS, 91128 Palaiseau cedex, France

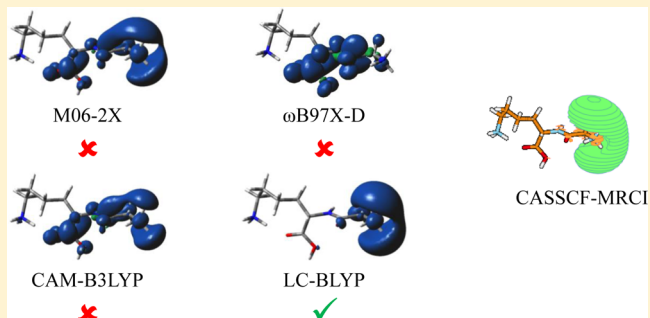
[‡]Laboratoire CEISAM, UMR CNRS 6230, Université de Nantes, 2 rue de la Houssinière - BP 92208, 44322 Nantes cedex 3, France

[§]Institut Universitaire de France, 103 bd Saint-Michel, F-75005 Paris Cedex 05, France

^{||}Service de Chimie quantique et Photophysique, Université Libre de Bruxelles, CP160/09, 50 av. F.D. Roosevelt, 1050 Bruxelles, Belgium

Supporting Information

ABSTRACT: We assess the pros and cons of a large panel of DFT exchange-correlation functionals for the prediction of the electronic structure of hydrogen-rich peptide radicals formed after electron attachment on a protonated peptide. Indeed, despite its importance in the understanding of the chemical changes associated with the reduction step, the question of the attachment site of an electron and, more generally, of the reduced species formed in the gas phase through electron-induced dissociation (ExD) processes in mass spectrometry is still a matter of debate. For hydrogen-rich peptide radicals in which several positive groups and low-lying π^* orbitals can capture the incoming electron in ExD, inclusion of full Hartree–Fock exchange at long-range interelectronic distance is a prerequisite for an accurate description of the electronic states, thereby excluding several popular exchange-correlation functionals, e.g., B3LYP, M06-2X, or CAM-B3LYP. However, we show that this condition is not sufficient by comparing the results obtained with asymptotically correct range-separated hybrids (M11, LC-BLYP, LC-BPW91, ω B97, ω B97X, and ω B97X-D) and with reference CASSCF-MRCI and EOM-CCSD calculations. The attenuation parameter ω significantly tunes the spin density distribution and the excited states vertical energies. The investigated model structures, ranging from methylammonium to hexapeptide, allow us to obtain a description of the nature and energy of the electronic states, depending on (i) the presence of hydrogen bond(s) around the cationic site(s), (ii) the presence of π^* molecular orbitals (MOs), and (iii) the selected DFT approach. It turns out that, in the present framework, LC-BLYP and ω B97 yields the most accurate results.



INTRODUCTION

Electron capture dissociation (ECD)^{1,2} and electron transfer dissociation (ETD)³ are recent fragmentation techniques that possess strong potential for the analysis of both peptides and proteins.^{4–6} In ECD and ETD, multiply protonated peptides are partially reduced by electron capture and transfer, respectively, and are subsequently converted from even-electron closed-shell species, to cation-radical intermediates that fragment mainly through N–C_α bond cleavage,⁷ leading to *c/z* fragments⁵ that are specific to these methods. The labile post-translational modifications are well-preserved during the fragmentation process,^{8–13} which is a great advantage of these methods, compared to more-standard techniques, such as collision-induced dissociation (CID). Since the reaction mechanism remains unclear, efficient empiric models able to predict the fragmentation of peptides are not available, which severely restricts the automatic determination of the peptide and protein primary structure information on the basis of the sole recorded fragmentation's spectrum. To date, several mechanisms have

been proposed, which could be classified by the attachment site of the incoming electron resulting in a charge-reduced cation-radical intermediate. This intermediate can be also described as an hydrogen-rich peptide–cation radical.¹⁴ Several electron attachment sites have been proposed:

- (i) one of the charged sites (N-terminal amine group or a basic amino-acid lysine, arginine, or histidine side chain) of the multiply protonated peptides;^{1,15–17}
- (ii) a hydrogen bond between backbone carbonyl and nitrogen groups;¹⁸ or
- (iii) an amide π^* -orbital,^{19–21} producing a charge-stabilized amide anion-radical intermediate in an electronic excited state (ES) but also possibly in the ground state (GS).^{22,23}

In all cases, a homolytic N–C_α bond cleavage occurs either before or after proton and/or hydrogen migration. Other

Received: April 9, 2014

Published: June 26, 2014

fragmentation pathways than N–C_α bond cleavage have also been observed experimentally.^{24–34}

Understanding the radiation damage process has motivated extensive theoretical and experimental works devoted to the electron attachment in biological molecules. [For recent reviews, see refs 35 and 36.] For positively charged isolated peptides, a model based on *ab initio* calculations has been proposed.^{37–39} This model allows one to analyze both the electron attachment and intramolecular electron transfer from ground-state and excited-Rydberg orbitals to the amide π*-orbital, based on their principal quantum number, size, and energy. In that framework, the accurate description of the electronic structure of charge-reduced peptides in both the GS and ES is a critical prerequisite for understanding the mechanism of fragmentation in ECD and ETD. Previous computational works on related systems mainly used the B3LYP exchange-correlation DFT functional for the GS and its time-dependent density functional theory (TD-B3LYP) framework for the ESs.^{22,40–48} Other DFT functionals, such as M06-2X and CAM-B3LYP, have also been applied in recent studies of hydrogen-rich peptide radicals.^{23,48–50} In a recent study, we have shown that DFT functionals that do not include full Hartree–Fock exchange (X^{HF}) at long-range interelectronic distance are unable to properly describe the GS electronic structure of the charge-reduced peptide cation radicals.⁵¹ Indeed, because of the self-interaction error, conventional DFT functionals yield an overly disperse spin density after addition or removal of an electron from closed-shell systems⁵² or show an excessive charge-transfer when describing radical-molecule interactions.⁵³ Only HF and post-HF methods, DFT functionals with 100% X^{HF} , and range-separated hybrid (RSH) functionals with correct asymptotic behavior provide an accurate description, in terms of both radical-cation intermolecular interaction energy and localization of spin density. Similar trends have been reported for the prediction of the spin density of organometallic species.⁵⁴ An inaccurate characterization of the spin localization could be a major problem for describing electron paramagnetic resonance (EPR) properties, because spin density is an essential ingredient in accurate EPR calculations. Contrary to the GS of hydrogen-rich peptide radicals for which computational methods have been probed,⁵¹ ESs have not been the subject of benchmark studies to determine which method describes them accurately. In addition, the natures and energies of the latter remain, to the best of our knowledge, unexplored with RSHs methods. In a charge-reduced peptide, it can be postulated that the electron is localized on the charged site with the highest electron affinity; however, the energy required to promote the electron to the other cationic site(s) or to an amide π*-orbital remains unknown. It is well-established that global and range-separated functionals (RSHs) can yield very different TD-DFT results.⁵⁵ Most of the numerous existing TD-DFT and *ab initio* benchmark studies focus on the excitations energies of closed-shell molecules including medium-sized⁵⁶ to large-sized⁵⁷ unsaturated organic molecules or transition-metal complexes.⁵⁸

In the present contribution, a large panel of exchange-correlation DFT functionals is used to investigate both the GS and ESs of radicals in the TD-DFT framework, and the TD-DFT results are benchmarked using reference data obtained with the CASSCF-MRCI wave function method as well as with the equation-of-motion coupled-cluster approach (EOM-CCSD) approach. Several chemical models of increasing complexity are studied (see Figure 1). First, we examine neutral radicals, including a NH₃ group either free (methylammonium **1**[•]) or implied in a hydrogen bond to an amide carbonyl group

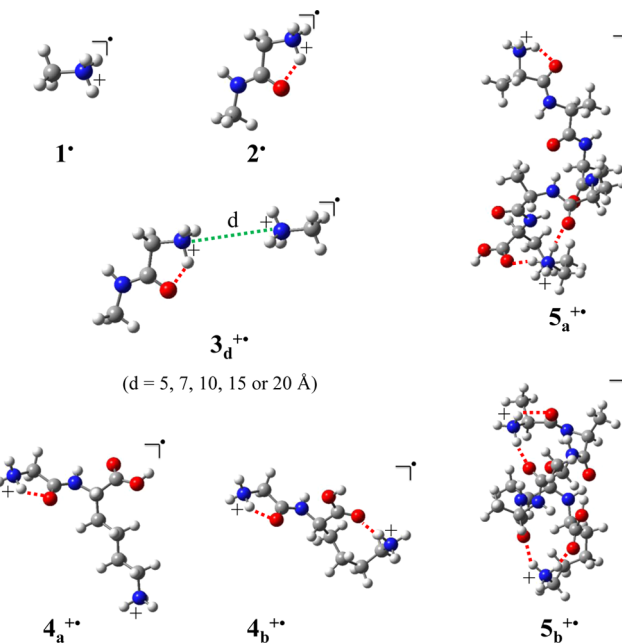


Figure 1. Studied model systems. Intramolecular hydrogen bonds to the ammonium group are depicted with red dashes.

(protonated glycine amide **2**[•]). Next, we combine these molecules to build the charge-reduced cation-radical peptide model **3**_d^{•+} including two NH₃ groups separated by a fixed distance d ($d = 5, 7, 10, 15$, or 20 Å). Finally, we extend our studies to real monoreduced diprotonated peptides. This includes both the dipeptide GlyLys, for which two conformations presenting different intramolecular hydrogen bonds have been computed (models **4**_a^{•+} and **4**_b^{•+}),⁴² and the hexapeptide Ala₅Lys (conformation models **5**_a^{•+} and **5**_b^{•+}) studied recently by Wodrich and co-workers.¹⁵

METHODS

All DFT and TD-DFT calculations have been performed with the Gaussian 09 program.⁵⁹ In this work, vertical reduction have been considered to avoid the complexity of considering simultaneously several ES geometries. Therefore, geometries used for all radicals correspond to the optimized structures of the nonreduced molecules. They have been obtained at the M06/6-311++G(d,p) level for **1**[•] and **2**[•], or taken from the literature for **3**_d²⁺,⁵¹ **4**_a²⁺/**4**_b²⁺,⁴² and **5**_a²⁺/**5**_b²⁺.¹⁵ A large panel of DFT functionals has been applied for these calculations. They can be classified into three categories: (a) the RSHs CAM-B3LYP,⁶⁰ HISSbPBE,⁶¹ ωB97X-D,⁶² ωB97X,⁶³ ωB97,⁶³ LC-BLYP,^{64,65} LC-BPW91,^{64,65} and M11;⁶⁶ (b) functionals including 100% X^{HF} , that is, M06-HF,^{67,68} and HFLYP;^{69,70} and (c) conventional pure and hybrid functionals, such as BLYP,^{69–71} B3LYP,^{69,72} M06,⁷³ BH&HLYP,⁷⁴ and M06-2X.⁷³ RSHs present a growing fraction of X^{HF} with increasing interelectronic separation, whereas the amount of X^{HF} is constant in all other methods (see Table 1). In all RSHs but HISSbPBE, the increased rate of X^{HF} is directly governed by the attenuation parameter ω , according to the scheme of eq 1:

$$\frac{1}{r_{12}} = \frac{\text{erf}(\omega r_{12})}{r_{12}} + \frac{1 - \text{erf}(\omega r_{12})}{r_{12}} \quad (1)$$

where erf is the error function and r_{12} is the interelectronic distance ($r_{12} = |r_1 - r_2|$). The larger the ω value, the faster the

Table 1. Mean Absolute Deviations (in eV) of the Absolute and Relative Vertical Excitation Energies for $\mathbf{1}^\bullet$ and $\mathbf{2}^\bullet$

functional	methods		MAD(E) ^c		MAD(ΔE) ^d		MAD _{average}
	n (%) ^a	ω ^b (a.u.)	1^\bullet	2^\bullet	1^\bullet	2^\bullet	
BLYP	0		0.14	0.44	0.24	0.31	0.28
B3LYP	20		0.10	0.27	0.18	0.20	0.19
M06	27		0.40	0.39	0.30	0.25	0.33
BH&HLYP	50		0.06	0.09	0.10	0.04	0.07
M06-2X	54		0.12	0.10	0.19	0.15	0.14
HISB-PBE	0–60–0	0.84/0.20 ^e	0.14	0.21	0.17	0.07	0.15
CAM-B3LYP	19–65	0.33	0.03	0.06	0.07	0.17	0.08
ω B97X-D	22.2–100	0.20	0.05	0.13	0.11	0.31	0.15
ω B97X	15.77–100	0.30	0.05	0.13	0.10	0.29	0.14
M11	42.8–100	0.25	0.44	0.22	0.25	0.17	0.27
ω B97	0–100	0.30	0.06	0.10	0.08	0.25	0.12
LC-BLYP	0–100	0.47	0.04	0.11	0.07	0.23	0.11
LC-BPW91	0–100	0.47	0.09	0.19	0.16	0.42	0.22
M06-HF	100		0.15	f	0.18	f	0.17
HFLY ^g	100		0.05	0.10	0.07	0.22	0.11
HF			0.14	0.09	0.10	0.24	0.14
EOM-CCSD			0.01	0.03	0.01	0.07	0.03

^aExact exchange percentage for DFT methods. ^bAttenuation parameters for long-range corrected functional. ^cMean absolute deviations of the TD-DFT vertical excitation energies (MAD(E)), relative to CASSCF-MRCI ones. ^dMean absolute deviations of the TD-DFT energy gaps between excited states (ESs). $\Delta E = E(\text{ES}_{i+1}^X) - E(\text{ES}_i^X)$; $X = 1, 2$; $i = 1–5$ for $\mathbf{1}^\bullet$ and $i = 1–2$ for $\mathbf{2}^\bullet$. ^e ω at short range (ω_{SR})/ ω at long range (ω_{LR}); the rate of X^{HF} is governed by these parameters according to: $1/r_{12} = [(1 - \text{erf}(\omega_{\text{SR}}r_{12}))/r_{12}] + (\text{erf}(\omega_{\text{LR}}r_{12}))/r_{12} + \{[1 - \text{erf}(\omega_{\text{LR}}r_{12})] - [1 - \text{erf}(\omega_{\text{SR}}r_{12})]\}/r_{12}$. ^fNo data available. ^gFunctional including full- X^{HF} part (no local and nonlocal exchange functional) and the Lee–Yang–Parr correlation functional. Obtained with G09 keywords and iop: “BLYP iop(3/76=0000010000) iop(3/77=0720008000) iop(3/78=0810010000)”.

transition from Kohn–Sham exchange (X^{KS}) to X^{HF} . The change between X^{KS} and X^{HF} differs for HISB-PBE, which possesses X^{HF} at middle range but only X^{KS} at short range and long range. It is well-known that the parameter ω can be adjusted to obtain a better correlation between theory and experience, either empirically⁷⁵ or following the optimal tuning approach recently developed by Baer and co-workers.^{76–80} In this approach, ω is not a universal constant but rather a system-specific range-separation parameter that satisfies to the best possible degree the ionization potential theorem.⁸¹ The optimally tuned range separated hybrid functionals have been shown, for example, to outperform many of the most efficient functionals for excited-state transition energies.⁸² For all cases, low-energy ES of hydrogen-rich peptide radicals correspond to the excitation of a single electron. This assumption was confirmed by CASSCF-MRCI and EOM-CCSD calculations (*vide infra*). Consequently, the nature of both the GS and the ESs could be either described by the singly occupied molecular orbital (SOMO) of the corresponding state, or by the spin density distribution. This last description is more convenient for TD-DFT calculations for which, in most cases, several vacant MOs significantly contribute to the description of ESs. Vertical excited-state energies and molecular spin densities of the ground and excited states have been computed using DFT and TD-DFT calculations. All calculations on radicals have been performed with the 6-311+ $+G(2d,p)$ atomic basis set. Their shapes were visualized applying a contour threshold of 0.001 a.u. Atomic spin densities have been calculated using the natural population analysis (NPA) method.⁸³

Because of the need to ensure the quality of our reference data for benchmarking the DFT performances, two high-level *ab initio* methods, including CASSCF-MRCI and EOM-CCSD, have been used. Multiconfiguration *ab initio* calculations on $\mathbf{1}^\bullet$, $\mathbf{2}^\bullet$, $\mathbf{3}_d^{+\bullet}$, and $\mathbf{4}_{a/b}^{+\bullet}$ have been performed using the same 6-311+ $+G(2d,p)$ atomic basis set. These complete active space self-

consistent field (CASSCF)⁸⁴ calculations have been performed in which the molecular orbitals playing an active role in the description of the ground and low-lying excited states were optimized. A state-averaging procedure has been used to optimize a common molecular orbital basis set describing the electronic states of the molecules. Main configuration state functions (CSFs) defining the low-lying states have been taken into account in a restricted active orbital space correlating a minimal number of electrons. In order to account for the remaining dynamical correlation, the CASSCF calculations have been followed by internally contracted multireference configuration interaction (MRCI) calculations.⁸⁵ All multiconfiguration *ab initio* calculations were performed with the MOLPRO program package.⁸⁶ The size of the active orbital space is defined by the standard notation $(n,m)_x$, indicating that n electrons are distributed among m molecular orbitals, with x being the number of states involved in the state averaging procedure. The choice of this active space is a key issue, because of both the required computer time and the sensitivity of the MRCI step to its size. It has been postulated in the literature⁴² that all low-lying excited states of hydrogen-rich peptide radicals correspond to excitation of the single electron. To validate this assumption and to exclude the possibility of multielectron excitation, CASSCF-MRCI calculations with an active space including one or five electrons in five orbitals were performed for $\mathbf{3}_5^{+\bullet}$ (see Table S1 in the Supporting Information (SI)). Equal excitation energies obtained from $(1,5)_3$ and $(5,5)_3$ active spaces justify, in the following, the use of active space including only one electron. Similarly, the influence of the number of molecular orbitals in the active space, as well as the number of states involved in the state averaging procedure, has been evaluated for $\mathbf{1}^\bullet$, $\mathbf{2}^\bullet$, $\mathbf{3}_5^{+\bullet}$, and $\mathbf{3}_{10}^{+\bullet}$. In all cases, the first excitation energies are similar, with a larger deviation of 0.04 eV for the second excited state of $\mathbf{2}^\bullet$ (see Table S1 in the SI). Consequently, minimal active orbital spaces have been used in CASSCF calculations: $(1,10)_7$ for $\mathbf{1}^\bullet$ and $\mathbf{2}^\bullet$

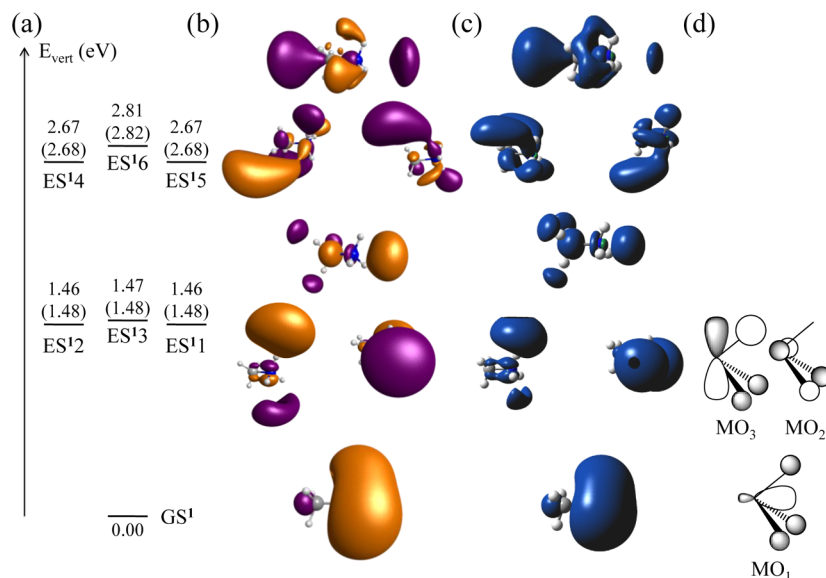


Figure 2. Vertical electronic states of $\mathbf{1}^{\bullet}$: (a) CASSCF-MRCI and EOM-CCSD (in bracket) energies, (b) CASSCF-MRCI SOMO, (c) LC-BLYP and TD-LC-BLYP spin density distributions of the ground and excited states, and (d) SALC-MOs from $\sigma_{\text{N}-\text{H}}^*$ orbitals in a XH_3 -type molecule ($\text{X} = \text{N}$) with a pyramidal geometry.

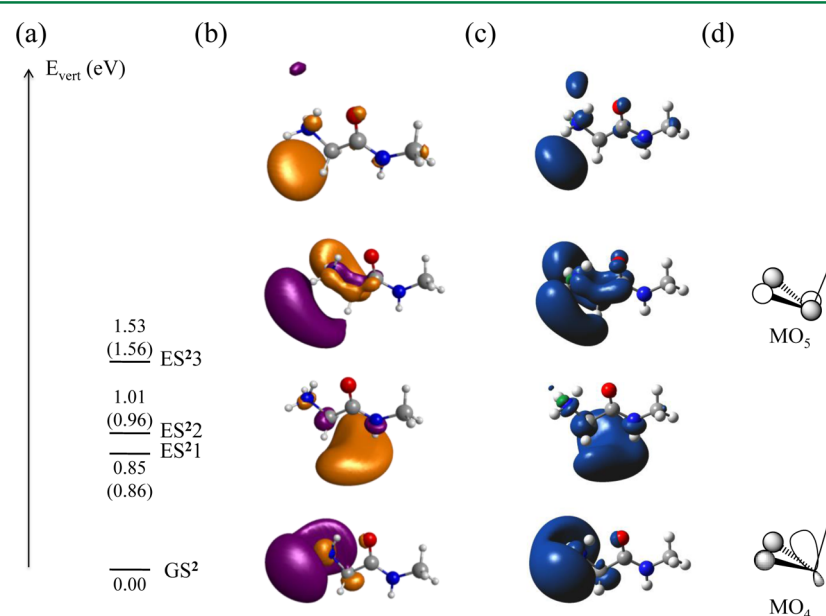


Figure 3. Vertical electronic states of $\mathbf{2}^{\bullet}$: (a) CASSCF-MRCI and EOM-CCSD (in bracket) energies, (b) CASSCF-MRCI SOMO, (c) LC-BLYP and TD-LC-BLYP spin density distributions of the ground and excited states, and (d) SALC-MOs from $\sigma_{\text{N}-\text{H}}^*$ orbitals in a bend XH_2 -type molecule ($\text{X} = \text{N}$).

and $(1,3)_3$ for $3_d^{+•}$ and $4_{a/b}^{+•}$. These spaces are defined by the highest occupied molecular orbital (HOMO) and the lowest unoccupied molecular orbitals (LUMO to LUMO+8 for $\mathbf{1}^{\bullet}$ and $\mathbf{2}^{\bullet}$, and LUMO and LUMO+1 for $3_d^{+•}$ and $4_{a/b}^{+•}$) in which one electron is distributed to form the CASSCF wave functions. These wave functions provided the smaller multiconfigurational description of the seven lowest states of the $\mathbf{1}^{\bullet}$ and $\mathbf{2}^{\bullet}$ systems and of the three lowest states for the $3_d^{+•}$ and $4_{a/b}^{+•}$. For $3_d^{+•}$ and $4_{a/b}^{+•}$, a significant amount of computer time is required for variationally optimizing the 33 and 55 closed-shell orbitals, respectively, in addition to the active orbitals. For this reason, we decided to freeze the 16 and 28 lowest occupied molecular orbitals for $3_d^{+•}$ and $4_{a/b}^{+•}$, respectively, arising from the 1s and 2s orbitals of O, C, and N atoms that were optimized at the SCF

level. The state-averaged CASSCF calculations with the minimal active orbital spaces were performed as a preliminary orbital optimization step to prepare for the MRCI calculations. The multireference wave function used in the MRCI calculations exactly corresponds to its CASSCF counterpart. All single and double excitations from the active orbitals to the external orbital space were included in the MRCI expansion whose size reached 10^6 , 10^6 , 10^7 , and 10^8 contracted CSFs, for $\mathbf{1}^{\bullet}$, $\mathbf{2}^{\bullet}$, $3_d^{+•}$, and $4_{a/b}^{+•}$, respectively. This level of calculation, noted CASSCF-MRCI in the following, takes into account both dynamic and static correlation effects of the active electrons providing an accurate representation of the electronic states of the chemical models. All MRCI energies include the Davidson correction for unlinked quadruple excitations.⁸⁷ This correction was calculated with a

relaxed multireference function as implemented in MOLPRO. The SOMO of each state can be visualized, but atomic spin densities are not available.

To further guarantee the reliability and accuracy of our CASSCF-MRCI reference calculations, relative excited-state energies were evaluated with the equation-of-motion coupled cluster method in the singles and doubles approximation (EOM-CCSD).⁸⁸ In this method, the ES wave function is generated from the coupled-cluster singles and doubles reference (CCSD) wave function of the ground state. EOM-CCSD calculations have been performed for **1[•]**, **2[•]**, and **3_d⁺** with the 6-311++G(2d,p) basis set used for other methods. Because of the well-known sensitivity of the basis set to EOM-CCSD results, comparison have been performed by using the aug-cc-pVTZ basis for **1[•]** and **2[•]**. The variations, which remain low (see Table S2 in the SI), confirm the relevance of using the 6-311++G(2d,p) basis set. GS molecular parameters (molecular orbitals and atomic spin density) are computed at the CCSD level of theory. In all cases, ESs result from the excitation of the electron located in the SOMO of the GS. In most cases, several vacant molecular orbitals (MOs) significantly contribute to the description of ESs, which makes difficult to determine the nature of these ESs.

RESULTS AND DISCUSSION

Benchmarks on Hydrogen-Rich Neutral Radicals. We started our study with the small neutral models **1[•]** and **2[•]** that

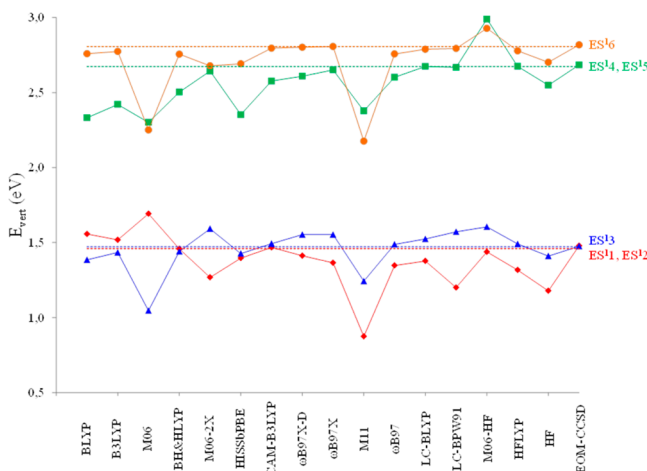


Figure 4. Vertical excitation energies of **1[•]** obtained at the TD-DFT and EOM-CCSD levels. The dotted line corresponds to the CASSCF-MRCI reference.

include a single NH₃ group. For these models, belonging to the C₃ and C_s point group, respectively, a chemically intuitive description of the electronic states could be achieved. Furthermore, they correspond to models for which conventional DFT should be able to describe the GS accurately, contrary to models including two NH₃ groups.⁵¹ Fifteen DFT functionals have been used on these models to assess their accuracy, in terms of absolute and relative energies of the first ESs, as well as spin densities.

As expected, for all methods, the single electron is unequivocally located on the charged group for both the GS of **1[•]** (noted GS¹) and **2[•]** (noted GS²). The electronic structures obtained at the CASSCF-MRCI level are represented in Figures 2 (**1[•]**) and 3 (**2[•]**), respectively. For **1[•]**, we observed degeneracies of the first (ES¹1, ES¹2) and third (ES¹4, ES¹5) ESs, because of

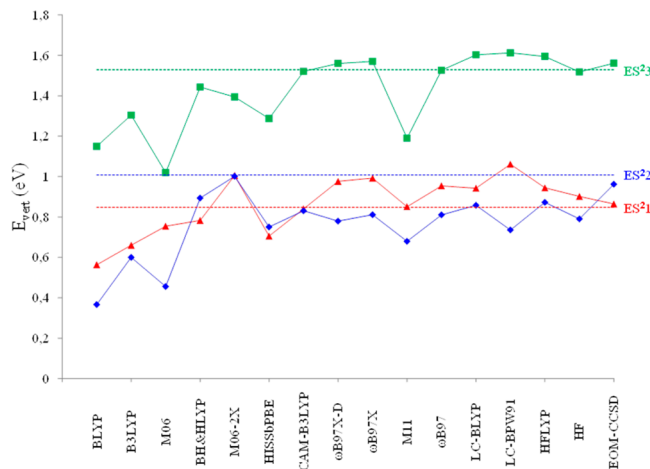


Figure 5. Vertical excitation energies of **2[•]** (see caption of Figure 4 for more details).

the C₃ symmetry axis. In addition, ES¹3 is close (0.01 eV) to the two former ESs. The shape of the SOMO of the GS¹, ES¹1, and ES¹2, is clearly reminiscent of the traditional antibonding molecular orbitals (MO₁, MO₂, and MO₃) of XH₃-type molecules with a pyramidal geometry. GS¹ corresponds to the in-phase combination of the three σ_{N-H}* orbitals (MO₁ in Figure 2), whereas ES¹1 and ES¹2 can be represented by the two other symmetry-adapted linear combinations (SALCs, MO₂, and MO₃) of these σ_{N-H}* orbitals. The SOMO in ES¹3-ES¹6 are mainly located on the CH₃ group, and could be described using both the σ_{N-C}* orbital and the SALCs resulting from the three σ_{C-H}* orbitals. The inclusion of a peptide bond, leading to **2[•]**, modifies the nature of electronic states, because of (i) the formation of a hydrogen bond between the amide CO and the NH₃ groups; (ii) the lowering of the point group symmetry from C₃ to C_s and; (iii) the emergence of low-energy vacant molecular orbitals (antisymmetric amide π* and symmetric amide σ_{N-H}*). The intramolecular hydrogen bond induces an energy increase of the associated σ_{N-H}* orbital. Therefore, in GS², the single electron is located only on the two free σ_{N-H}* orbitals (MO₄). Their antibonding combination (MO₅), observed for ES¹1, corresponds to ES²2 in **2[•]**. We underline that the contribution of the amide π* orbital is very low in ES²2. ES²1, which is located slightly below ES²2 (0.85 eV vs 1.01 eV), can be described as the in-phase combination between σ_{C-H}* (ES¹3) and the amide σ_{N-H}* orbitals. This analysis suggests that, contrary to the traditional point of view in ECD and ETD,³⁸ the electron is not trapped into a Rydberg orbital on positive moieties of protonated amines but is rather located on their antibonding σ_{N-H}* orbitals, and that the amide π*-orbital is less accessible than an appropriate combination of the σ*-orbitals. EOM-CCSD calculations (Figures 2 and 3) give very similar transition energies for both **1[•]** and **2[•]**, confirming the relevance of the CASSCF-MRCI data.

We have assessed the accuracies reached with several DFT approaches for **1[•]** and **2[•]**. The selected criteria were the absolute transition energies (from the GS), and the splitting between the excited states, considering the CASSCF-MRCI results as reference. The nature of all ESs has been established by comparison of the CASSCF-MRCI SOMO and the TD-DFT spin density distribution (see Figures 2 and 3), and reasonable match was obtained in the majority of cases. The TD-DFT vertical energies are compared to their CASSCF-MRCI counter-

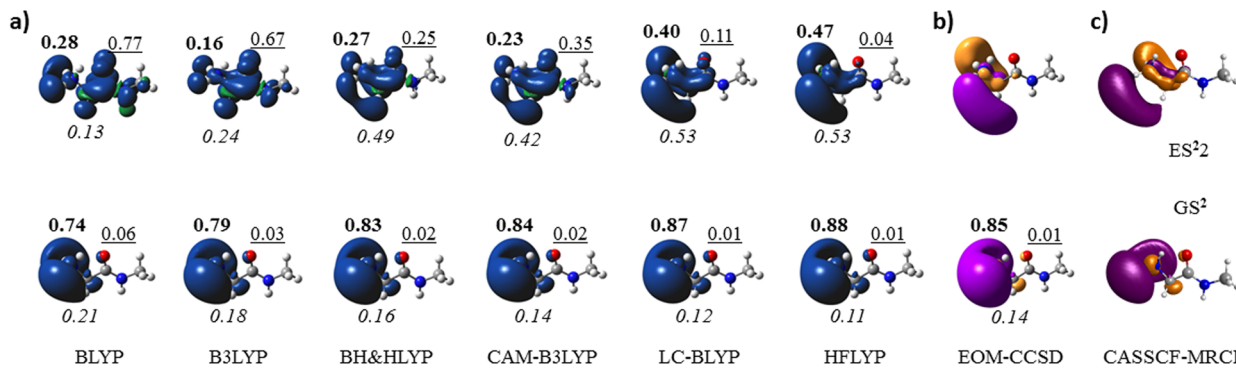


Figure 6. (a) Spin densities of GS² and ES² for DFT methods. (b) CCSD SOMO of GS² and vacant MO with the largest contribution (0.887) in ES² at the EOM-CCSD level. (c) CASSCF-MRCI SOMO of GS² and ES². Atomic spin densities of NH₃, CH₂, and CONHCH₃ are given in bold, italic, and underlined fonts, respectively.

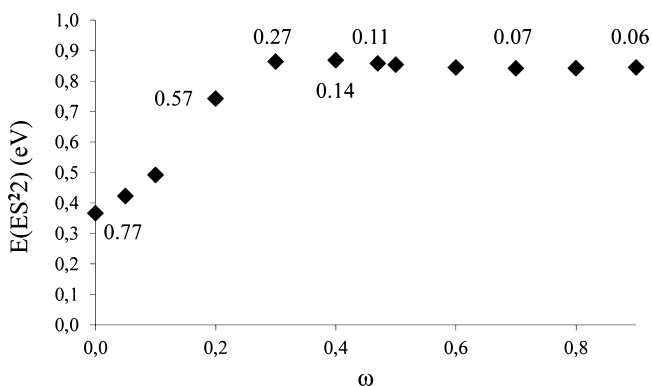


Figure 7. Effects of the attenuation parameter ω on the vertical excitation energy to ES² and its spin density located on the CONHCH₃ amide group (values in electron) using tuned LC-BLYP.

Table 2. States of Reduced 3_{10}^{+*} Obtained with ω B97X-D and LC-BLYP Functionals and *Ab Initio* Methods

state	electronic structure similar to	Vertical Excitation Energies (eV)			
		LC-BLYP	ω B97X-D	EOM-CCSD ^a	CASSCF-MRCI
GS ^{3d(d=10)}	GS ¹	0.00	0.00	0.00	0.00
ES ^{3d(d=10)} 1	GS ²	0.56	0.55	0.56	0.57
ES ^{3d(d=10)} 2	ES ¹²	1.43	1.46	1.53	1.51
ES ^{3d(d=10)} 3	ES ¹¹	1.45	1.47	1.54	1.52
ES ^{3d(d=10)} 4	ES ²	1.58	1.33	1.58	1.61

^aThe exact nature of the ESs could not be checked, as several vacant MOs contribute to their description.

parts in Figures 4 and 5. Qualitatively, for **1**[•], all RSHs and methods including 100% X^{HF} reproduce the ES ordering obtained with CASSCF-MRCI, but for M11 and M06-HF, which interchange two states (ES¹⁴, ES¹⁵) with ES¹⁶. All conventional functionals, except M06-2X, interchange (ES¹¹, ES¹²) with ES¹³, but this effect is probably not very significant, because of the energetic proximity of these states at the CASSCF-MRCI level (see above). M06 also inverts ES¹⁴ and ES¹⁵ with ES¹⁶. For **2**[•], all functionals (but HISSbPBE and BH&HLYP) invert the first and second ESs. The mean absolute deviations (MAD) of the TD-DFT vertical excitation energies, MAD(E), as well as of the relative state ES energy deviations, MAD(ΔE), are both reported in Table 1. As mentioned above, EOM-CCSD data are very similar to CASSCF-MRCI ones, leading to very small

MAD values between these methods. The largest MAD(E) values are observed for M06 and M11 for **1**[•] and **2**[•], respectively, whereas most functionals yield mean deviations smaller than 0.1 eV, the most accurate being CAM-B3LYP, BH&HLYP, LC-BLYP, HFLYP, ω B97, ω B97X, ω B97X-D, and M06-2X, as well as the Hartree–Fock (HF) method. BLYP, B3LYP, HISSbPBE, and LC-BPW91 functionals have a MAD(E) close to 0.1 eV for **1**[•] but this value is significantly larger for **2**[•]. The trends for the MAD(ΔE) of **1**[•] are similar to their MAD(E) counterparts. In contrast, for **2**[•], the trends differ for these two criteria. Indeed, the MAD(ΔE) of BH&HLYP and HISSbPBE are very small, indicating a good match with CASSCF-MRCI, whereas most functionals have MAD(ΔE) values close to 0.2 eV, except LC-BPW91, BLYP, ω B97X-D, and ω B97X, which yield larger deviations. By averaging these deviations for both **1**[•] and **2**[•], we can conclude that (i) the most accurate methods, in terms of energies, are BH&HLYP, CAM-B3LYP, LC-BLYP, HFLYP, and ω B97, and (ii) those providing the less-satisfying results are BLYP, M06, M11, and LC-BPW91.

The LC-BLYP spin densities are represented in Figures 2 and 3. For all ground and excited states, the shape of the SOMO and the spin density are very similar. The same qualitative agreement is obtained for all others methods used, except for, on the one hand, HF (see ES¹⁵ in Figure S1 in the SI) and, on the other hand, M06-HF, M11, M06-2X, and M06, which give large spin contamination for ESs of both **1**[•] and **2**[•], inducing unreasonable spin density distributions. Significant quantitative differences between the electronic states are observed for system **2**[•], as the spin density of many states is more delocalized with DFT, and more specifically with conventional functionals, than with CASSCF-MRCI SOMO or EOM-CCSD data. This is illustrated for both GS² and ES² in Figure 6. While the ground-state densities are qualitatively similar for all methods, quantitative estimation of the atomic spin density shows however that the smaller the X^{HF} , the larger the electron delocalization on the amide moiety. This effect is more pronounced for ES². With conventional functionals, the spin density is delocalized on the entire molecule, mainly on the NH₃ and CO groups. An increase of X^{HF} induces a localization of the spin density on the CH₂-NH₃ termination, as observed with CASSCF-MRCI and EOM-CCSD. The undue delocalization obtained with low X^{HF} functionals can be correlated with smaller excitation energies, thereby explaining the inaccuracy of these approaches from both qualitative and quantitative points of view (Figure 5).

With RSH, the same trends are observed. CAM-B3LYP, which does not include full X^{HF} at long range, shows a larger spin

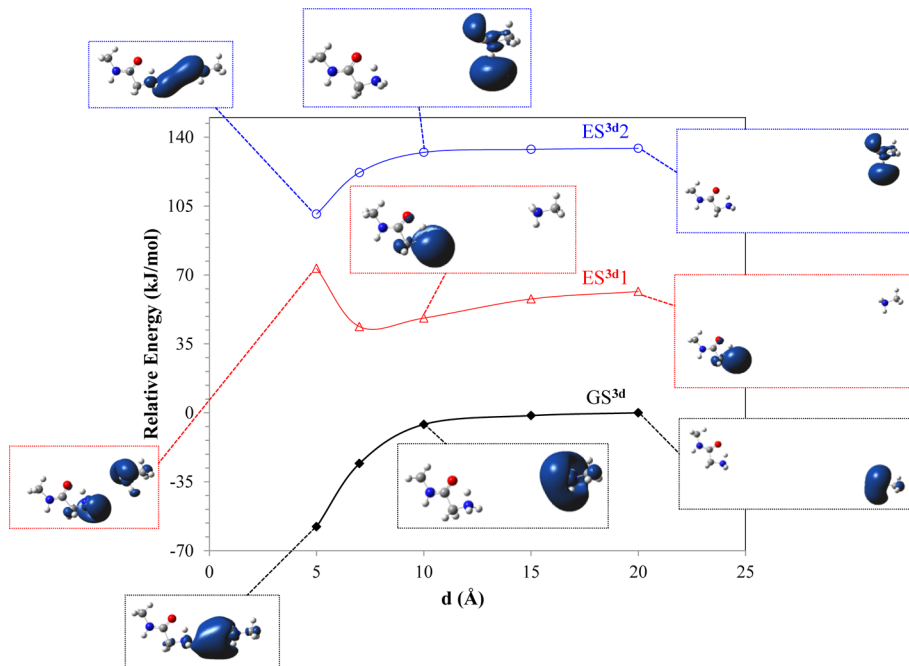


Figure 8. Effect of the N···N distance on the electronic structure of $3_d^{+•}$ ($d = 5, 7, 10, 15, 20 \text{ \AA}$). LC-BLYP spin densities and relative energies are given. Relative energies are calculated in comparison to the energy of $\text{GS}^{3d(d=20)}$.

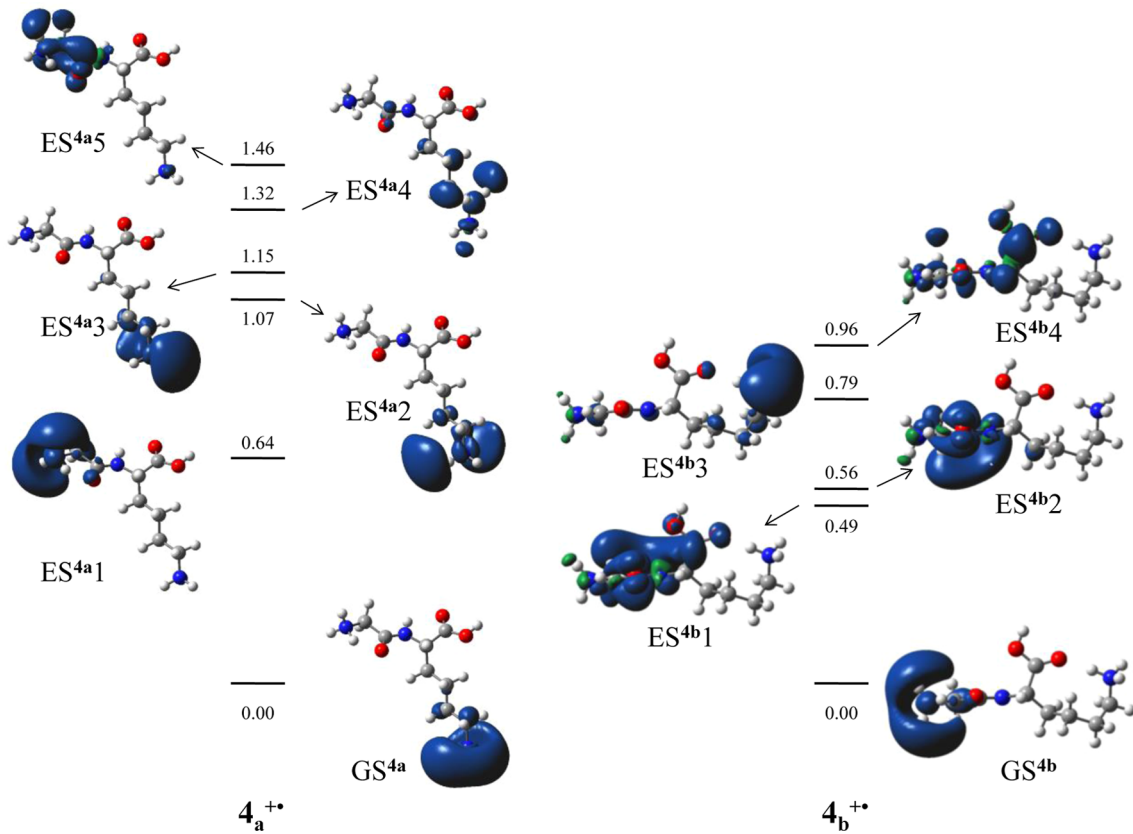


Figure 9. Spin densities and vertical excitation energies (eV) of ground and excited states of $4_a^{+•}$ and $4_b^{+•}$ at the LC-BLYP level.

delocalization on the amide group than LC-BLYP. The comparison of ω B97, ω B97X, and ω B97X-D results (see Figure S2 in the SI) indicates a stronger delocalization for the last-mentioned, in accordance with its smaller attenuation parameter ω (all three functionals presenting an asymptotically correct

X^{HF}). To ascertain this hypothesis, we have modified the parameter ω of LC-BLYP and investigated the energy and spin density of ES^{22} (see Figure 7). Similar calculations have been achieved for ω B97X-D, ω B97X, and ω B97 (see Figure S3 in the SI). For ω values between 0 and 0.3, the smaller the ω , the

Table 3. Atomic Spin Densities of Ground and Excited States of $4_a^{+\bullet}$ and $4_b^{+\bullet}$

	N-term ^a	CH ₂ ^b	CO ^c	HN-C _α ^d	Lys _{sc} ^e	C-term ^f	SOMO ^g
GS ^{4a}							
B3LYP	0.29	0.06	0.06	0.00	0.61	0.01	
M06-2X	0.04	0.01	0.01	0.00	0.94	0.00	
CAM-B3LYP	0.13	0.03	0.01	0.00	0.83	0.00	
ω B97X-D	0.00	0.00	0.00	0.00	1.00	0.00	
ω B97X-D ^h	0.00	0.00	0.00	0.00	1.00	0.00	
ω B97	0.00	0.00	0.00	0.00	1.00	0.00	
LC-BLYP	0.00	0.00	0.00	0.00	1.00	0.00	
HFLYP ⁱ	0.00	0.00	0.00	0.00	1.00	0.00	
ES ^{4a} 1							
B3LYP	0.36	0.06	-0.02	0.01	0.63	-0.01	
M06-2X	0.08	0.02	0.01	0.01	0.95	0.00	
CAM-B3LYP	0.12	0.02	-0.01	0.00	0.88	0.00	
ω B97X-D	0.68	0.17	0.10	0.02	0.06	0.01	
ω B97X-D ^h	0.73	0.16	0.04	0.01	0.07	0.00	
ω B97	0.74	0.16	0.03	0.01	0.08	0.00	
LC-BLYP	0.78	0.16	0.02	0.01	0.04	0.00	
HFLYP ⁱ	0.78	0.16	0.02	0.01	0.05	0.00	
ES ^{4a} 2							
B3LYP	0.00	0.11	0.46	0.03	0.59	0.01	
M06-2X	-0.01	0.14	0.64	0.04	0.34	0.00	
CAM-B3LYP	-0.02	0.10	0.58	0.03	0.70	0.01	
ω B97X-D	0.16	0.14	0.62	0.04	0.05	0.01	
ω B97X-D ^h	0.02	0.01	0.00	0.00	0.98	0.00	
ω B97	0.02	0.01	0.00	0.00	0.98	0.00	
LC-BLYP	0.01	0.00	0.00	0.00	0.98	0.00	
HFLYP ⁱ	0.01	0.00	0.00	0.00	0.99	0.00	
GS ^{4b}							
B3LYP	0.32	0.12	0.07	0.06	0.20	0.23	
M06-2X	0.51	0.18	0.05	0.05	0.04	0.16	
CAM-B3LYP	0.38	0.20	0.07	0.08	0.05	0.21	
ω B97X-D	0.02	0.06	0.31	0.10	0.01	0.51	
ω B97X-D ^h	0.77	0.19	0.02	0.01	0.00	0.01	
ω B97	0.76	0.20	0.02	0.01	0.00	0.01	
LC-BLYP	0.74	0.22	0.02	0.02	0.01	0.01	
HFLYP ⁱ	0.00	0.00	0.01	0.04	0.01	0.93	

^aNH₃ terminal group. ^bGlycine C_αH₂ group. ^cGlycine CO group. ^dLysine HN-C_α group. ^eLysine (CH₂)₄NH₃ side chain. ^fCOOH terminal group.

^gCASSCF-MRCI SOMO. ^h ω B97X-D with a modified parameter $\omega = 0.30$. ⁱSee footnote g in Table 1.

smaller the transition energies and the larger the spin density on the amide group. For $\omega \geq 0.3$ ($\omega \geq 0.4$), the transition energy (spin density) becomes nearly independent of the attenuation parameter.

Considering the results obtained for relative energies, MADs, and spin densities, we concluded that LC-BLYP, ω B97, and HFLYP produce the most satisfactory results. To study the larger systems $3_d^{+\bullet}$, $4_a^{+\bullet}$, $4_b^{+\bullet}$, $5_a^{+\bullet}$, and $5_b^{+\bullet}$, we have used these methods as well as the commonly used B3LYP, M06-2X, ω B97X-D, and CAM-B3LYP hybrid functionals in order to confirm the trends obtained on model systems. The best match with CASSCF-MRCI and EOM-CCSD was obtained with LC-BLYP, which is therefore mainly used in the following (see the SI for additional results).

Studies of Hydrogen-Rich Peptide Cation Radicals. We first focus on $3_d^{+\bullet}$, which can be viewed as the combination of 1^+ , 2^+ , and one additional electron. $3_d^{+\bullet}$ is a simplified model of real hydrogen-rich peptide cation radicals. For example, $3_{10}^{+\bullet}$ is an analogue of $4_a^{+\bullet}$ as they present the same noncovalent interactions around the NH₃ groups and similar N···N distances (10.0 and 9.9 Å, respectively). Clearly, the electronic states of

$3_{10}^{+\bullet}$ can be viewed as the combination of those of 1^+ and 2^+ (see Table 2, Figure 8, and Figure S4 in the SI), the electron being localized on one of the two subgroups. Note that the fourth ES of $3_{10}^{+\bullet}$ (= ES^{3d(d=10)}4 in Table 2) is overstabilized with ω B97X-D, because the delocalization of the electron on the amide group is exaggerated, compared to LC-BLYP. This effect induces a reversal in the ES ordering. Similar incorrect results, indicating a too easily accessible amide π^* -orbital, are therefore expected for other peptides with methods including too small ω value and/or less than 100% X^{HF} at long range. Vertical excitation energies computed at the EOM-CCSD and CASSCF-MRCI levels give very good agreement with the LC-BLYP values (Table 2).

The variation of the distance between the ammonium groups allows us to study the influence of this chemical parameter on both the energy and spin density of each state. Results for GS^{3d}, ES^{3d}1 and ES^{3d}2 are discussed here and those of ES^{3d}3 and ES^{3d}4 are reported in the SI. As expected, the energetic ranking and the nature of the ground and excited states obtained with LC-BLYP agree with the CASSCF-MRCI reference. Similar agreement is obtained with EOM-CCSD for the vertical excitation energies, even if larger values are observed in some cases, in particular for

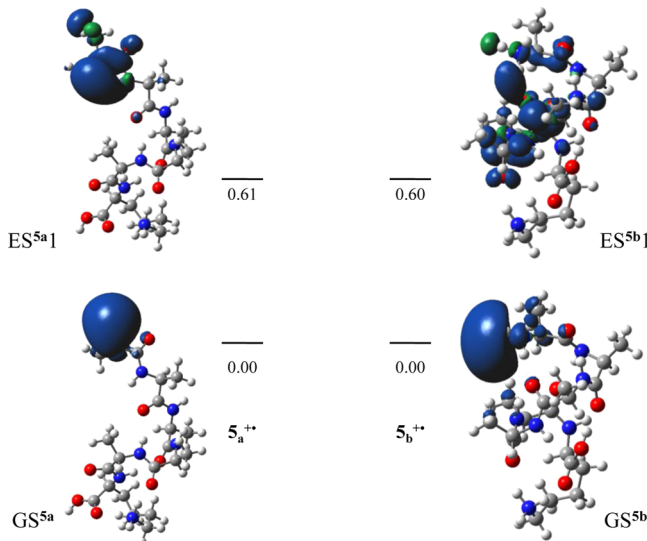


Figure 10. LC-BLYP spin densities and vertical excitation energies of the GS and ES1 of $5_a^{+\bullet}$ and $5_b^{+\bullet}$.

$3_s^{+\bullet}$ (see the SI). The electronic structure of $3_d^{+\bullet}$ remains unchanged for $d \geq 10 \text{ \AA}$, as shown in Figure 8. For the small distances, states of $3_d^{+\bullet}$ are obtained by symmetry-adapted linear combinations of the electronic states of 1^\bullet and 2^\bullet . In the ground state, the electron is delocalized between the two ammonium groups, corresponding to the in-phase combination of GS¹ and GS², whereas ES^{3d1} corresponds to the out-of-phase combination. Similarly, ES^{3d2} is the in-phase mix of ES¹¹ and ES²². The nature of these states explains their stabilization (in-phase combination) or destabilization (out-of-phase combination), compared to the situation observed for $d \geq 10 \text{ \AA}$.

We used LC-BLYP to investigate the electronic structure of $4_a^{+\bullet}$ and $4_b^{+\bullet}$ (Figure 9). As expected, $4_a^{+\bullet}$ behaves similarly to $3_{10}^{+\bullet}$. The lowest electronic states present spin densities localized on one of the ammonium group. The first excited state in which the amide π^* -orbital is populated is ES^{4a5} at 1.46 eV, whereas ES^{4a1} at 0.64 eV shows very low spin density on the amide moiety. Once again, ω B97X-D, CAM-B3LYP, B3LYP,⁴² and M06-2X (see the SI) give a populated amide π^* -orbital for an ES of much lower energy (at 0.99, 0.61, 0.40, and 0.47 eV, respectively), in sharp disagreement with the CASSCF-MRCI reference, which give results similar to LC-BLYP. Comparison of the atomic spin densities for the GS and the first ESs of $4_a^{+\bullet}$ (Table 3) quantitatively confirm the performance of the functionals.

For $4_b^{+\bullet}$, another low-energy conformation of the GlyLys dipeptide that includes one additional hydrogen bond between the COOH and the NH₃ group of the lysine, the nature of the electronic states is completely modified. Indeed, in the ground state GS^{4b}, the electron is located on the N-terminal ammonium, similar to what is found with the first excited state (ES^{4a1}) of $4_a^{+\bullet}$. The state corresponding to GS^{4a} is pushed up to ES^{4b3} due to the additional hydrogen bond. The lowest excited state in which the electron is localized in the amide π^* -orbital appears 0.49 eV above the ground-state, and is therefore significantly more accessible than in $4_a^{+\bullet}$. Among the other tested functionals (see Table 3 and the SI), only ω B97 gives the same ground state as LC-BLYP and CASSCF-MRCI. CAM-B3LYP, B3LYP, and M06-2X lead to an extensive delocalization of the spin density over the N-term ammonium, the C-term carboxylic group, and the amide group of the dipeptide in GS^{4b}. The HFLYP ground

state presents the unpaired electron located in the carboxylic group rather than on the N-term NH₃. Eventually, because of the overstabilization of the electronic states including partly filled amide π^* -orbitals, ω B97X-D inverts GS^{4b} and ES^{4b1}. This reversal can be solved by increasing the attenuation parameter from 0.2 a.u. to 0.3 a.u. (functional noted ω B97X-D*), which restores accurate results for both $4_b^{+\bullet}$ and $4_a^{+\bullet}$.

Are the above conclusions on the nature of the electronic states and on the reliability of DFT functionals in that framework maintained for longer, more-realistic, peptides? To explore this issue, our study has been extended to the hexapeptide Ala₃Lys, which has been examined recently in a joint theoretical-experimental study and was shown to undergo cleavages of the N–C_α bond with ECD and ETD.¹⁵ The spin density of the GS^{5a/b} and the ES^{5a/b1} for two low-energy conformations are given in Figure 10. In $5_a^{+\bullet}$, the N-term ammonium is isolated from the other groups while the ammonium group of the lysine side chain is hydrogen-bonded to both the COOH and a CO group of one amide. $5_b^{+\bullet}$ also includes a hydrogen bond between the N-term ammonium and one CO. In both cases, at the LC-BLYP level (Figure 10), as well as for ω B97 and HFLYP (see the SI), the ground state corresponds to the addition of the single electron to the N-term ammonium, the charged site with the larger electron affinity, that is, with the weaker hydrogen bonds. The spin density in ES^{5a1} is located around the amide bond closest to the N-term, whereas a spin-density delocalization over several amide π^* -orbitals is predicted for ES^{5b1}. ω B97X-D, CAM-B3LYP, and B3LYP give similar results for $5_a^{+\bullet}$ with, however, larger spin density delocalization, and smaller transition energy in particular for B3LYP. As for $4_b^{+\bullet}$, ground and excited states of $5_b^{+\bullet}$ are not correctly described by these methods as well as by M06-2X, confirming all the trends noted previously.

CONCLUSIONS

Using CASSCF-MRCI results as benchmarks, as well as EOM-CCSD calculations, we have benchmarked a panel of exchange-correlation functionals in the framework of the description of the ground and excited states of hydrogen-rich peptide cation radicals. Fifteen functionals have been assessed considering two criteria on small chemical models: (i) energetics, including the ordering of excited states, vertical excitation energies and the excited states splitting; and (ii) spin densities of both ground and excited states. All conventional DFT approaches fail to pass these two tests, whereas LC-BLYP, ω B97, and HFLYP provide the best agreement with CASSCF-MRCI and EOM-CCSD. Notably, in range-separated hybrids, the attenuation parameter ω can significantly modify both the spin density distribution and the vertical excitation energies even when 100% X^{HF} is included at long-range interelectronic distance.

Seven functionals have been applied on hydrogen-rich di- and hexa-peptide cation radicals, confirming both the robustness of ω B97 and LC-BLYP, as well as the failure of the popular B3LYP, M06-2X, ω B97X-D approaches, and, to a smaller extent, CAM-B3LYP. Increasing the size of the studied systems as well as changing their conformation allowed us to understand the nature and the order of the electronic states as a function of noncovalent interactions around the ammonium groups. It turned out that the number of hydrogen bonds on the ammonium groups is a decisive chemical parameter that guides the electronic structure of hydrogen-rich peptide radicals.

■ ASSOCIATED CONTENT

Supporting Information

Complete refs 59 and 86. Assessment of the active space size for CASSCF-MRCI calculations and influence of the basis set on EOM-CCSD results. HF electronic structure of **1⁺**. Effects of X^{HF} and attenuation parameter on the GS² and ES² properties using ωB97, ωB97X, and ωB97X-D. LC-BLYP relative energies and spin densities for ES^{3d}3 and ES^{3d}4. Relative energies and SOMOs of 3_d⁺⁺, 4_a⁺⁺, and 4_b⁺⁺ obtained at the CASSCF-MRCI and EOM-CCSD levels. The ωB97X-D* ($\omega = 0.3$) electronic structure of 4_a⁺⁺ and 4_b⁺⁺. Spin densities and vertical excitation energies of 4_a⁺⁺, 4_b⁺⁺, 5_a⁺⁺, and 5_b⁺⁺ obtained with ωB97X-D, ωB97, HFLYP, CAM-B3LYP, B3LYP, and M06-2X. This material is available free of charge via the Internet at <http://pubs.acs.org>.

■ AUTHOR INFORMATION

Corresponding Author

*Tel.: +33 (0)1 69 33 48 34. Fax: +33 (0)1 69 33 48 03. E-mail: gilles.frison@polytechnique.org.

Notes

The authors declare no competing financial interest.

■ ACKNOWLEDGMENTS

V.R., D.J., and G.F. gratefully acknowledge financial support from GDR 3533 "EMIE". D.J. acknowledges the European Research Council (ERC) and the *Région des Pays de la Loire* for financial support in the framework of a Starting Grant (Marches-278845) and a *recrutement sur poste stratégique*, respectively. This work was performed using HPC resources from GENCI-CINES (Grant No. x2013087105).

■ REFERENCES

- (1) Zubarev, R. A.; Kelleher, N. L.; McLafferty, F. W. *J. Am. Chem. Soc.* **1998**, *120*, 3265–3266.
- (2) McLafferty, F. W.; Horn, D. M.; Breuker, K.; Ge, Y.; Lewis, M. A.; Cerdá, B.; Zubarev, R. A.; Carpenter, B. K. *J. Am. Soc. Mass Spectrom.* **2001**, *12*, 245–249.
- (3) Syka, J. E.; Coon, J. J.; Schroeder, M. J.; Shabanowitz, J.; Hunt, D. F. *Proc. Natl. Acad. Sci. U.S.A.* **2004**, *101*, 9528–9533.
- (4) Zubarev, R. A.; Horn, D. M.; Fridriksson, E. K.; Kelleher, N. L.; Kruger, N. A.; Lewis, M. A.; Carpenter, B. K.; McLafferty, F. W. *Anal. Chem.* **2000**, *72*, 563–573.
- (5) Cooper, H. J.; Hakansson, K.; Marshall, A. G. *Mass Spectrom. Rev.* **2005**, *24*, 201–222.
- (6) Mikesh, L. M.; Ueberheide, B.; Chi, A.; Coon, J. J.; Syka, J. E. P.; Shabanowitz, J.; Hunt, D. F. *Biochim. Biophys. Acta* **2006**, *1764*, 1811–1822.
- (7) Zubarev, R. A.; Haselmann, K. F.; Budnik, B.; Kjeldsen, F.; Jensen, F. *Eur. J. Mass Spectrom.* **2002**, *8*, 337–349.
- (8) Stensballe, A.; Jensen, O. N.; Olsen, J. V.; Haselmann, K. F.; Zubarev, R. A. *Rapid Commun. Mass Spectrom.* **2000**, *14*, 1793–1800.
- (9) Kellerher, N. L.; Zubarev, R. A.; Bush, K.; Furie, B.; Furie, B. C.; McLafferty, F. W.; Walsh, C. T. *Anal. Chem.* **1999**, *71*, 4250–4253.
- (10) Mirgorodskaya, E.; Roepstorff, P.; Zubarev, R. A. *Anal. Chem.* **1999**, *71*, 4431–4436.
- (11) Shi, S. D.; Hemling, M. E.; Carr, S. A.; Horn, D. M.; Lindh, I.; McLafferty, F. W. *Anal. Chem.* **2001**, *73*, 19–22.
- (12) Sze, S. K.; Ge, Y.; Oh, H. B.; McLafferty, F. W. *Proc. Natl. Acad. Sci. U.S.A.* **2002**, *99*, 1774–1779.
- (13) Ge, Y.; Lawhorn, B. G.; ElNaggar, M.; Strauss, E.; Park, J. H.; Begley, T. P.; McLafferty, F. W. *J. Am. Chem. Soc.* **2002**, *124*, 672–678.
- (14) Turecek, F.; Julian, R. R. *Chem. Rev.* **2013**, *113*, 6691–6733.
- (15) Wodrich, M.; Zhurov, K.; Vorobyev, A.; Ben Hamidane, H.; Corminboeuf, C.; Tsbybin, Y. O. *Phys. Chem. B* **2012**, *116*, 10807–10815.
- (16) Wodrich, M. D.; Zhurov, K. O.; Corminboeuf, C.; Tsbybin, Y. O. *Phys. Chem. B* **2014**, *118*, 2985–2992.
- (17) Zhurov, K. O.; Wodrich, M. D.; Corminboeuf, C.; Tsbybin, Y. O. *Phys. Chem. B* **2014**, *118*, 2628–2637.
- (18) Patriksson, A.; Adams, C.; Kjeldsen, F.; Raber, J.; van der Spoel, D.; Zubarev, R. A. *Int. J. Mass Spectrom.* **2006**, *248*, 124–135.
- (19) Syrstad, E. A.; Turecek, F. *J. Am. Soc. Mass Spectrom.* **2005**, *16*, 208–224.
- (20) Sawicka, A.; Skurski, P.; Hudgins, R. R.; Simons, J. *J. Phys. Chem. B* **2003**, *107*, 13505–13511.
- (21) Sobczyk, M.; Anusiewicz, I.; Berdys-Kochanska, J.; Sawicka, A.; Skurski, P.; Simons, J. *J. Phys. Chem. A* **2005**, *109*, 250–258.
- (22) Turecek, F.; Chung, T. W.; Moss, C. L.; Wyer, J. A.; Ehlerding, A.; Holm, A. I. S.; Zettergren, H.; Nielsen, S. B.; Hvelplund, P.; Chamot-Rooke, J.; Bythell, B.; Paizs, B. *J. Am. Chem. Soc.* **2010**, *132*, 10728–10740.
- (23) Turecek, F.; Moss, C. L.; Chung, T. W. *Int. J. Mass Spectrom.* **2012**, *330*–332, 207–219.
- (24) Breuker, K.; Oh, H. B.; Horn, D. M.; Cerdá, B. A.; McLafferty, F. W. *Eur. J. Mass Spectrom.* **2002**, *8*, 177–180.
- (25) Cooper, H. J.; Hudgins, R. R.; Håkansson, K.; Marshall, A. G. *J. Am. Soc. Mass Spectrom.* **2002**, *13*, 241–249.
- (26) Cooper, H. J. *J. Am. Soc. Mass Spectrom.* **2005**, *16*, 1932–1940.
- (27) Fung, Y. M.; Chan, T. W. *J. Am. Soc. Mass. Spectrom.* **2005**, *16*, 1523–1535.
- (28) Lee, S.; Chung, G.; Kim, J.; Oh, H. B. *Rapid Commun. Mass Spectrom.* **2006**, *20*, 3167–3175.
- (29) Liu, H.; Håkansson, K. *J. Am. Soc. Mass Spectrom.* **2007**, *18*, 2007–2013.
- (30) Haselmann, K. F.; Schmidt, M. *Rapid Commun. Mass Spectrom.* **2007**, *21*, 1003–1008.
- (31) Falth, M.; Savitski, M. M.; Nielsen, M. L.; Kjeldsen, F.; Andren, P. E.; Zubarev, R. A. *Anal. Chem.* **2008**, *80*, 8089–8094.
- (32) van der Rest, G.; Hui, R.; Frison, G.; Chamot-Rooke, J. *J. Am. Soc. Mass Spectrom.* **2011**, *22*, 1631–1644.
- (33) Marek, A.; Pepin, R.; Peng, B.; Laszlo, K. J.; Bush, M. F.; Tureček, F. *J. Am. Soc. Mass Spectrom.* **2013**, *24*, 1641–1653.
- (34) Kalapothakis, J. M. D.; Berezovskaya, Y.; Zampronio, C. G.; Faull, P. A.; Barran, P. E.; Cooper, H. J. *Chem. Commun.* **2014**, *50*, 198–200.
- (35) Alizadeh, E.; Sanche, L. *Chem. Rev.* **2012**, *112*, 5578–5602.
- (36) Gu, J.; Leszczynski, J.; Schaefer, H. F. *Chem. Rev.* **2012**, *112*, 5603–5640.
- (37) Neff, D.; Simons, J. *J. Phys. Chem. A* **2009**, *114*, 1309–1323.
- (38) Simons, J. *Chem. Phys. Lett.* **2010**, *484*, 81–95.
- (39) Simons, J. *J. Am. Chem. Soc.* **2010**, *132*, 7074–7085.
- (40) Chamot-Rooke, J.; Malosse, C.; Frison, G.; Tureček, F. *J. Am. Soc. Mass Spectrom.* **2007**, *18*, 2146–2161.
- (41) Frison, G.; van der Rest, G.; Turecek, F.; Besson, T.; Lemaire, J.; Maitre, P.; Chamot-Rooke, J. *J. Am. Chem. Soc.* **2008**, *130*, 14916–14917.
- (42) Turecek, F.; Chen, X.; Hao, C. *J. Am. Chem. Soc.* **2008**, *130*, 8818–8833.
- (43) Panja, S.; Brøndsted Nielson, S.; Hvelplund, P.; Tureček, F. *J. Am. Soc. Mass Spectrom.* **2008**, *19*, 1726–1742.
- (44) Jensen, C. S.; Holm, A. I. S.; Zettergren, H.; Overgaard, J. B.; Hvelplund, P.; Brøndsted Nielson, S. *J. Am. Soc. Mass Spectrom.* **2009**, *20*, 1881–1889.
- (45) Sohn, C. H.; Chung, C. K.; Yin, S.; Ramachandran, P.; Loo, J. A.; Beauchamp, J. L. *J. Am. Chem. Soc.* **2009**, *131*, 5444–5459.
- (46) Bythell, B. *J. Phys. Chem. A* **2013**, *117*, 1189–1196.
- (47) Maclot, S.; Rangama, J.; Brøndsted Nielson, S.; Pouilly, J. C. *Int. J. Mass Spectrom.* **2013**, *337*, 1–11.
- (48) Pepin, R.; Laszlo, K. J.; Peng, B.; Marek, A.; Bush, M. F.; Tureček, F. *J. Chem. Phys. A* **2014**, *118*, 308–324.
- (49) Moss, C. L.; Liang, W.; Li, X.; Tureček, F. *J. Am. Soc. Mass Spectrom.* **2012**, *23*, 446–459.
- (50) Ledvina, A. R.; Chung, T. W.; Hui, R.; Coon, J. J.; Tureček, F. *J. Am. Soc. Mass Spectrom.* **2012**, *23*, 1351–1363.

- (51) Gilson, A. I.; van der Rest, G.; Chamot-Rooke, J.; Kurlancheck, W.; Head-Gordon, M.; Jacquemin, D.; Frison, G. *J. Phys. Chem. Lett.* **2011**, *2*, 1426–1431.
- (52) (a) Lundberg, M.; Siegbahn, P. E. M. *J. Chem. Phys.* **2005**, *122*, 224103–224109. (b) Cohen, A. J.; Mori-Sánchez, P.; Yang, W. T. *Science* **2008**, *321*, 792–794.
- (53) Johnson, E. J.; Salamone, M.; Bietti, M.; DiLabio, G. A. *J. Phys. Chem. A* **2013**, *117*, 947–952.
- (54) (a) Conradie, J.; Ghosh, A. *J. Phys. Chem. B* **2007**, *111*, 12621–12624. (b) Boguslawski, K.; Jacob, C. R.; Reiher, M. *J. Chem. Theory Comput.* **2011**, *7*, 2740–2752.
- (55) (a) Leang, S. S.; Zahariev, F.; Gordon, M. S. *J. Chem. Phys.* **2012**, *136*, 104101–104112. (b) Laurent, A. D.; Jacquemin, D. *Int. J. Quantum Chem.* **2013**, *113*, 2019–2039 and references therein.
- (56) (a) Schreiber, M.; Silva-Junior, M. R.; Sauer, S. P. A.; Thiel, W. J. *Chem. Phys.* **2008**, *128*, 134110. (b) Silva-Junior, M. R.; Schreiber, M.; Sauer, S. P. A.; Thiel, W. J. *Chem. Phys.* **2008**, *129*, 104103.
- (57) Goerigk, L.; Grimme, S. *J. Chem. Phys.* **2010**, *132*, 184103.
- (58) (a) Vlcek, A.; Zalis, S. *Coord. Chem. Rev.* **2007**, *251*, 258–287. (b) Gonzalez, L.; Escudero, D.; Serrano-Andrés, L. *ChemPhysChem* **2012**, *13*, 28–51.
- (59) Frisch, M. J.; Trucks, G. W.; Schlegel, H. B.; Scuseria, G. E.; Robb, M. A.; Cheeseman, J. R.; Scalmani, G.; Barone, V.; Mennucci, B.; Petersson, G. A.; et al. *Gaussian 09, Revision B.01*; Gaussian, Inc.: Wallingford, CT, 2010.
- (60) Yanai, T.; Tew, D.; Handy, N. *Chem. Phys. Lett.* **2004**, *393*, 51–57.
- (61) (a) Henderson, T. M.; Izmaylov, A. F.; Scuseria, G. E.; Savin, A. J. *Chem. Phys.* **2007**, *127*, 221103. (b) Henderson, T. M.; Izmaylov, A. F.; Scuseria, G. E.; Savin, A. J. *Chem. Theory Comput.* **2008**, *4*, 1254–1262.
- (62) Chai, J. D.; Head-Gordon, M. *Phys. Chem. Chem. Phys.* **2008**, *10*, 6615–6620.
- (63) Chai, J. D.; Head-Gordon, M. *J. Chem. Phys.* **2008**, *128*, 084106–084115.
- (64) Likura, H.; Tsuneda, T.; Yanai, T.; Hirao, K. *J. Chem. Phys.* **2001**, *115*, 3540–3544.
- (65) Tsuneda, T.; Hirao, K. *WIREs Comput. Mol. Sci.* DOI: 10.1002/wcms.1178.
- (66) Peverati, R.; Truhlar, D. G. *J. Phys. Chem. Lett.* **2011**, *2*, 2810–2817.
- (67) Zhao, Y.; Truhlar, D. G. *J. Phys. Chem. A* **2006**, *110*, 5121–5129.
- (68) Zhao, Y.; Truhlar, D. G. *J. Phys. Chem. A* **2006**, *110*, 13126–13130.
- (69) Lee, C.; Yang, W.; Parr, R. G. *Phys. Rev. B* **1988**, *37*, 785–89.
- (70) Miehlich, B.; Savin, A.; Stoll, H.; Preuss, H. *Chem. Phys. Lett.* **1989**, *157*, 200–206.
- (71) Becke, A. D. *Phys. Rev. A* **1988**, *38*, 3098–100.
- (72) Becke, A. D. *J. Chem. Phys.* **1993**, *98*, 1372–77.
- (73) Zhao, Y.; Truhlar, D. G. *Theor. Chem. Acc.* **2008**, *120*, 215–241.
- (74) Becke, A. D. *J. Chem. Phys.* **1993**, *98*, 5648–5652.
- (75) Rabilloud, F. *J. Phys. Chem. A* **2013**, *117*, 4267–4278.
- (76) (a) Refaelly-Abramson, S.; Baer, R.; Kronik, L. *Phys. Rev. B* **2011**, *84*, 0751441–8. (b) Kronik, L.; Stein, T.; Refaelly-Abramson, S.; Baer, R. *J. Chem. Theory Comput.* **2012**, *8*, 1515–1531. (c) Refaelly-Abramson, S.; Sharifzadeh, S.; Govind, N.; Autschbach, J.; Neaton, J. B.; Baer, R.; Kronik, L. *Phys. Rev. Lett.* **2012**, *109*, 226405 1–6.
- (77) Karolewski, A.; Kronik, L.; Kümmel, S. *J. Chem. Phys.* **2013**, *138*, 204115 1–11.
- (78) Agrawal, P.; Tkatchenko, A.; Kronik, L. *J. Chem. Theory Comput.* **2013**, *9*, 3473–3478.
- (79) Moore, B., II; Autschbach, J. *J. Chem. Theory Comput.* **2013**, *9*, 4991–5003.
- (80) Sun, H.; Autschbach, J. *ChemPhysChem* **2013**, *14*, 2450–2461.
- (81) Baer, R.; Livshits, E.; Salzner, U. *Annu. Rev. Phys. Chem.* **2010**, *61*, 85–109.
- (82) Jacquemin, D.; Moore, B., II; Planchat, A.; Adamo, C.; Autschbach, J. *J. Chem. Theory Comput.* **2014**, *10*, 1677–1685.
- (83) Reed, A. E.; Weinstock, R. B.; Weinhold, F. *J. Chem. Phys.* **1985**, *83*, 735–746.
- (84) Roos, B. O.; Taylor, P. R.; Siegbahn, P. E. M. *Chem. Phys.* **1980**, *48*, 157–173.
- (85) (a) Knowles, P. J.; Werner, H. J. *Chem. Phys. Lett.* **1988**, *145*, 514–522. (b) Werner, H. J.; Knowles, P. J. *J. Chem. Phys.* **1988**, *89*, 5803–5814.
- (86) Werner, H. J.; Knowles, P. J.; Knizia, G.; Manby, F. R.; Schütz, M.; Celani, P.; Korona, T.; Lindh, R.; Mitrushenkov, A.; Rauhut, G.; et al. *Molpro, version 2010.1*, a package of ab initio programs, 2010. See <http://www.molpro.net>.
- (87) Langhoff, S. R.; Davidson, E. R. *Int. J. Quantum Chem.* **1974**, *8*, 61–72.
- (88) Stanton, J. F.; Bartlett, R. J. *J. Chem. Phys.* **1993**, *98*, 7029–7039.